Journal of Engineering Mathematics (2005) 51: 81–97

Flows of inelastic non-Newtonian fluids through arrays of aligned cylinders. Part 2. Inertial effects for square arrays

P.D.M. SPELT[1,2,3,*], T. SELERLAND[1,**], C.J. LAWRENCE[3] and P.D. LEE[2]
[1]*Centre for Composite Materials, Department of Aeronautics,* [2]*Department of Materials and* [3]*Department of Chemical Engineering, Imperial College London, United Kingdom*

Received 18 February 2004; accepted in revised form 14 May 2004

Abstract. Numerical simulations are presented for flows of inelastic non-Newtonian fluids through periodic arrays of aligned cylinders. The truncated power-law fluid model is used for the relationship between the viscous stress and the rate-of-strain tensor. Results for the drag coefficient for creeping flows of such fluids have been presented in a companion paper [1]. In this second part the effects of finite fluid inertia are investigated for flows through square arrays. It is shown that the Reynolds-number dependence of the drag coefficient of a cylinder in the array is of the form $C_d \equiv F/(\eta U) = k_0 + k_2 \mathrm{Re}^2 + ..$ for small values of the Reynolds number $\mathrm{Re} \equiv \rho a U/\eta$, where F is the drag force, U is the averaged velocity in the array, $\eta = K(U/a)^{n-1}$ is a viscosity scale with K and n the power-law coefficient and index and a the cylinder radius, and k_0 is the drag coefficient for creeping flows. The proportionality constant k_2 depends on the way the drag coefficient and the Reynolds number are defined. It is shown that the observed strong dependence of k_2 on n can almost be eliminated by using length scales different from a in the viscosity scales η used in the definition of Re and in the definition of the drag coefficient. Numerical simulation results are also presented for the velocity variance components. Results for flows at moderate Reynolds number, of order 100, are also presented; these are qualitatively similar to those for Newtonian fluids. The value of the Reynolds number beyond which the flow becomes unsteady was related to the Newtonian fluid case by rescaling. These results for moderate-Reynolds-number flow are compared against previously published experimental data.

Key words: inelastic non-Newtonian fluids, inertial effects, periodic cylinder arrays

1. Introduction

In a companion paper [1] we have presented numerical simulation results for the creeping flow of inelastic non-Newtonian fluids through arrays of cylinders. The effects of fluid inertia in these flows is the subject of this second part.

As is described in [1], the main issue is the determination of the drag coefficient for a cylinder in the array, and most early studies have been restricted to creeping flows of Newtonian fluids. More recently, flows with small-but-finite and intermediate Reynolds numbers $\mathrm{Re} = \rho a U/\mu$ have been studied, where ρ is the fluid viscosity, a is the cylinder radius, U is the averaged velocity in the array and μ is the fluid viscosity. Edwards *et al.* [2] and Ghaddar [3] calculated the on-axis flows (*i.e.*, transverse flows along an axis of the array) through periodic arrays of cylinders at intermediate Reynolds numbers. Koch and Ladd [4] presented

*Present address: School of Mathematical Sciences, University of Nottingham, Nottingham NG7 2RD, UK.
**Present address: CFD Recipes, Unit 171, Parkers House, 48 Regent Street, Cambridge CB2 1FD, UK.

a full investigation of the off-axis transverse flows through square arrays and the transverse flow through random arrays.

Koch and Ladd [4] showed that, for Newtonian flow at small Reynolds numbers, the first two terms in an expansion of the drag coefficient C_d of a cylinder in the array in Re are

$$C_d \equiv \frac{F}{\mu U} = k_0 + k_2 \mathrm{Re}^2 \qquad (\mathrm{Re} \ll 1), \tag{1}$$

where the coefficients k_0 and k_2 depend on the solid area fraction (ϕ) of the array and k_2 also depends on the angle θ between the mean flow direction and the axes of the array. This result is also more generally valid for the inertial correction to Darcy's law for flow through porous media [5]. Experiments on flow through porous media support an inertial correction that is linear in Re instead, but a transition between (1) and a linear regime is found at $\mathrm{Re} \approx 3$ for flow through periodic arrays of cylinders that are placed randomly in a unit cell of the array [4].

For Newtonian fluids, the dependence of the correction factor k_2 on ϕ is significant. At small ϕ, it is dominated by the fact that the drag coefficient for a single cylinder in an infinite medium does not satisfy (1), making k_2 singular at $\phi = 0$ and very large at small ϕ. For concentrated arrays, the fluid has to be squeezed through the narrow gaps between the cylinders, causing the drag force (both k_0 and k_2) to become very large and singular at closest packing (the area fraction at which the cylinders touch). Koch and Ladd [4] also showed that for small Reynolds numbers the mean flow direction is further away from the axes of the array than is the drag force.

In this paper, we resolve the form of the inertial correction to the drag coefficient for inelastic fluid flow through square arrays. In [1] it is shown that creeping flows through arrays of cylinders are dominated by shear, not extension. As in [1], we use the truncated power-law model for the relation between the viscous part of the local stress tensor τ_{ij} and the rate-of-strain tensor E_{ij} in the fluid [6, Chapter 4]:

$$\tau_{ij} = 2\eta E_{ij}, \tag{2}$$

with

$$E_{ij} = \frac{1}{2}\left(\frac{\partial V_i}{\partial x_j} + \frac{\partial V_j}{\partial x_i}\right), \tag{3}$$

and the effective viscosity

$$\eta = \begin{cases} K\Pi^{(n-1)/2} & \text{if} \quad \Pi \geq \dot{\gamma}_0^2, \\ \eta_0 & \text{if} \quad \Pi \leq \dot{\gamma}_0^2, \end{cases} \tag{4}$$

where $\dot{\gamma}_0 = (\eta_0/K)^{1/(n-1)}$ and $\Pi = 2E_{kl}E_{kl}$ is the second invariant of the rate-of-strain tensor (summation over the indices k and l is presumed). K and n are the power-law coefficient and index, respectively. The case of $n = 1$ corresponds to a Newtonian fluid; $n < 1$ provides a model of a pseudoplastic or shear-thinning fluid and $n > 1$ corresponds to a shear-thickening fluid. As in [1], we shall consider here the range $0{\cdot}5 \leq n \leq 1{\cdot}5$, and choose $\dot{\gamma}_0$ sufficiently small such that its value does not affect the results (corresponding to a power-law fluid model). Since the effective viscosity is no longer constant throughout the fluid, the Reynolds number

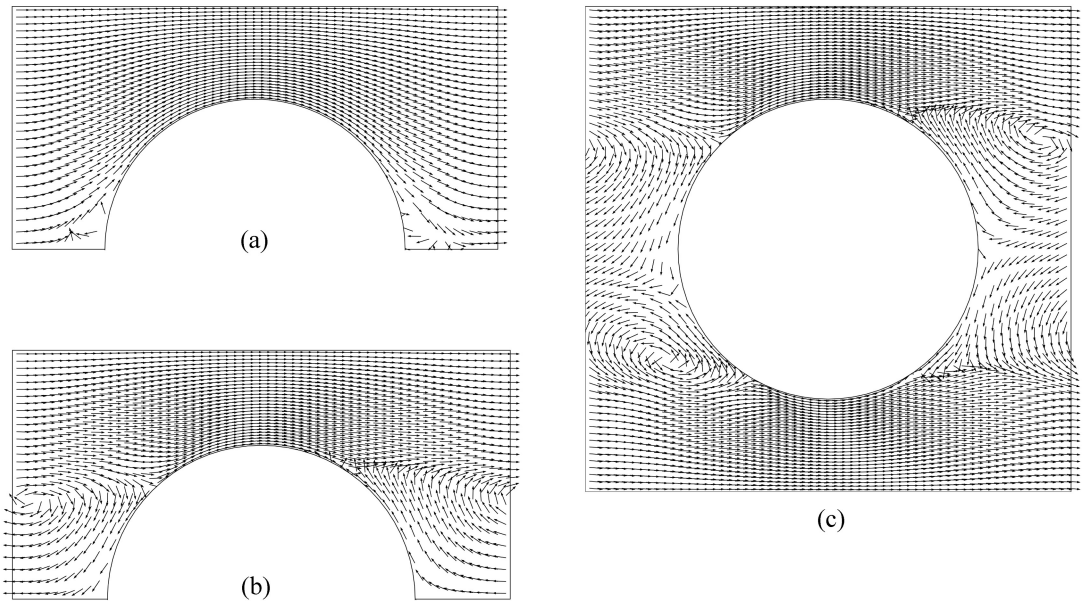

Figure 1. Velocity fields for on-axis flows of a shear-thinning fluid ($n = 0{\cdot}5$) at solid area fraction $\phi = 0{\cdot}3$, at different Reynolds numbers: (a), Re $= 0$, (b) Re $= 22{\cdot}5$ and (c), Re $= 31{\cdot}0$. The velocity field at Re $= 31{\cdot}0$ is unsymmetrical and unsteady. The arrows have uniform length and indicate only the direction of the velocity.

will be defined as $\mathrm{Re} = \rho a U/\eta$, where η is a viscosity scale that we choose initially equal to $\eta_a \equiv K(U/a)^{n-1}$. The drag coefficient C_d is defined by

$$F = C_d(\phi, n, \mathrm{Re}, \theta)\, \eta\, U. \tag{5}$$

The numerical method presented in [1] is used in this study. In Figure 1, resulting velocity fields are shown for three different Reynolds numbers where the power-law index is 0·5 and the solid area fraction 0·3. We see a symmetrical velocity field that is at steady state in the creeping-flow regime (Figure 1a). A breaking of the fore-aft asymmetry is seen in the steady-state result for a finite Reynolds number (Figure 1b). At the highest Reynolds number the recirculation zones between the cylinders have become unsteady (Figure 1c). Qualitatively similar behaviour was found in [4] for Newtonian fluid flow through square arrays.

On the other hand, the non-linear dependence of the stress tensor on the strain rate will cause the drag coefficient to differ from the Newtonian results, as is evident from [1]. Previous work on a related problem for finite Reynolds numbers has been reported in [7], where numerical simulation results are presented for the flow of power-law fluids past a single cylinder for three different Reynolds numbers (based on the cylinder diameter: $\mathrm{Re}_d = 5$, 20 and 40), with values of the power-law index n between 0·65 and 1·2 (at the highest Reynolds number $0{\cdot}95 \leq n \leq 1{\cdot}1$). The results from that study show a significant dependence of the drag coefficient on the power-law index.

Flows of inelastic non-Newtonian fluids through arrays of cylinders have been studied experimentally, motivated by finding a friction factor for heat exchangers that are used for non-Newtonian fluids. Adams and Bell [8] presented experimentally determined friction factors (which can be converted into drag coefficients for individual cylinders) for flows of CMC solutions through square arrays at solid area fraction $\phi = 0{\cdot}5$; other cylinder arrangements were also studied. CMC solutions are shear-thinning fluids, the power-law index of the solu-

tions used was in the range $0{\cdot}58 \leq n \leq 1$. Friction factor data were presented over a range of Reynolds numbers. Prakash, Gupta and Mishra [9] collected experimental data from various sources and developed a model, based on the flow through a channel of varying cross-section, in an attempt to collapse the data. More recently, Prasad and Chhabra [10] presented experimental data for flows of CMC solutions through triangular and staggered square arrays of cylinders for solid area fractions lower than those considered in [8].

In Section 2 we examine how the velocity field in the array changes with Reynolds number for different values of the power-law index, and how the drag coefficient C_d depends on the Reynolds number of the flow in general. In particular, we show that a relationship similar to (1) also holds for power-law fluids. Also, in Section 2 we present results for the drag coefficient for both on-axis and off-axis flows at small, but finite, Reynolds numbers. Values of the velocity variances for the corresponding cases are presented in Section 3. Results for flows at moderate Reynolds numbers, of order 100, are presented in Section 4.

2. First effects of inertia on the drag coefficient

2.1. Series expansion for finite-Reynolds-number flows of power-law fluids

In this section we demonstrate that a relationship similar to (1) also holds for the drag coefficient of power-law fluids. Koch and Ladd [4] proved (1) by considering a regular expansion of the velocity and pressure in the Reynolds number, and we shall follow their derivation here, but for power-law fluids.

Using the dimensionless position vector $\mathbf{x}^* = \mathbf{x}/a$, velocity vector $\mathbf{V}^*(\mathbf{x}^*) = \mathbf{V}/U$, and pressure $P^* = K^{-1}a^{-n}U^{-n}P$, the dimensionless equations of motion at steady state are

$$\frac{\partial V_j^*}{\partial x_j^*} = 0, \qquad \mathrm{Re}\frac{\partial}{\partial x_j^*}\left(V_i^* V_j^*\right) = -\frac{\partial P^*}{\partial x_i^*} + \frac{\partial \tau_{ij}^*}{\partial x_j^*}, \tag{6}$$

where

$$\tau_{ij}^* = 2^{(n+1)/2}(E_{kl}^* E_{kl}^*)^{(n-1)/2} E_{ij}^*, \qquad E_{ij}^* = \frac{1}{2}\left(\frac{\partial V_i^*}{\partial x_j^*} + \frac{\partial V_j^*}{\partial x_i^*}\right). \tag{7}$$

Introducing the expansions

$$\mathbf{V}^* = \mathbf{V}^{(0)} + \mathrm{Re}\mathbf{V}^{(1)} + \ldots \quad \text{and} \quad P^* = P^{(0)} + \mathrm{Re}\, P^{(1)} + \ldots \tag{8}$$

we have

$$\frac{\partial V_j^{(m)}}{\partial x_j^*} = 0 \qquad \text{for all } m, \tag{9}$$

$$0 = -\frac{\partial P^{(0)}}{\partial x_i^*} + 2^{(n+1)/2}\frac{\partial}{\partial x_j^*}\left((E_{kl}^{(0)} E_{kl}^{(0)})^{(n-1)/2} E_{ij}^{(0)}\right), \tag{10}$$

$$\begin{aligned}\frac{\partial}{\partial x_j^*}\left(V_i^{(0)} V_j^{(0)}\right) = {} & -\frac{\partial P^{(1)}}{\partial x_i^*} + 2^{(n+1)/2}\frac{\partial}{\partial x_j^*}\left((E_{kl}^{(0)} E_{kl}^{(0)})^{(n-1)/2} E_{ij}^{(1)}\right. \\ & \left. + (n-1)(E_{kl}^{(0)} E_{kl}^{(0)})^{(n-3)/2} E_{rs}^{(0)} E_{rs}^{(1)} E_{ij}^{(0)}\right).\end{aligned} \tag{11}$$

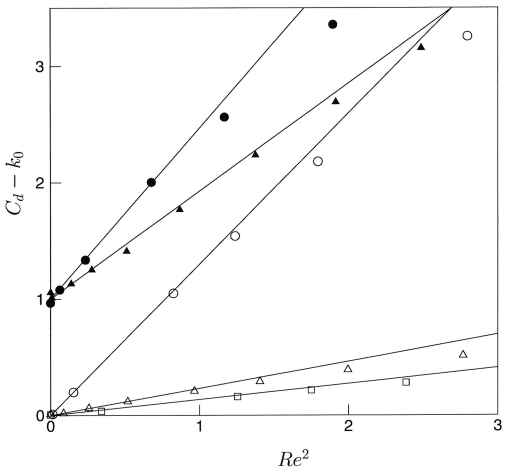

Figure 2. Inertial contribution $C_d - k_0$ to the drag coefficient as a function of Reynolds number for on-axis flow (open symbols) and off-axis flow at the symmetry angle $\theta = \pi/4$ (filled symbols). The lines indicate the asymptotic result (12). (□), $n = 0{\cdot}5$, $\phi = 0{\cdot}05$; (△,▲), $n = 0{\cdot}5$, $\phi = 0{\cdot}3$; (○,●), $n = 0{\cdot}5$, $\phi = 0{\cdot}5$. The data for off-axis flows are shifted vertically by one unit for clarity.

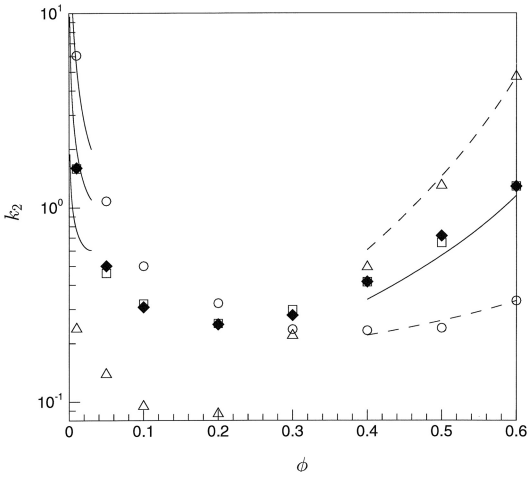

Figure 3. Variation of k_2 with solid area fraction ϕ at different values of the power-law index: (□), $n = 1$; (△), $n = 0{\cdot}5$ and (◯), $n = 1{\cdot}5$. The solid diamonds (⧫) are results for $n = 1$ by Koch and Ladd [4]. The solid lines at low solid fraction were obtained from (20) with $H = L_g$, and using $k_2(\phi, n = 1)$ from the dilute theory (14) by Koch and Ladd [4] for Newtonian fluids. The solid line at large ϕ indicates the lubrication theory by Koch and Ladd [4] for Newtonian fluids. The dashed lines are the lubrication scaling (13) where we have used the numerical simulation result at $\phi = 0{\cdot}6$ to obtain the proportionality constant.

In the $O(\mathrm{Re})$ momentum equation (11) we have used a Taylor series expansion to obtain the contribution from the viscous stress. As the local viscosity is a function of an invariant (which has reflectional symmetry) of the rate-of-strain tensor, the creeping-flow velocity field $\mathbf{V}^{(0)}$ is an even function of the position vector $\mathbf{x}^*$. Consequently, $P^{(0)}$ is an odd function of position. Then the left-hand side of (11) is odd so that $P^{(1)}$ is even and $\mathbf{V}^{(1)}$ is odd. Hence there is no contribution of $O(\mathrm{Re})$ to the drag. This argument can be repeated for the higher-order terms in the expansion and we conclude that

$$C_d(\phi, n, \mathrm{Re}, \theta) = k_0(\phi, n, \theta) + k_2(\phi, n, \theta)\mathrm{Re}^2 + \ldots, \qquad (Re \ll 1), \tag{12}$$

which is a generalisation of the result for Newtonian fluids ($n = 1$) derived in [4].

Our numerical simulations confirm (12). Examples are shown in Figure 2 for both on-axis and off-axis flows. Results for k_0 have already been presented in [1]; the main problem addressed in the rest of this section is therefore the determination of k_2.

At low solid area fractions the Reynolds number Re has to be very small in order to obtain k_2. To ensure that the flow approaches the creeping flow regime throughout the fluid the Reynolds number based on the distance between the cylinders should be small as well, requiring that $\mathrm{Re} \ll \phi^{n/2}$. On the other hand, the difference in drag coefficient for flows at very small Reynolds number can be dominated by numerical error. However, the dependence

of the drag coefficient on Reynolds number was gradual enough in all the cases simulated here so that it was not necessary to use values of Re between 0 and 0·1 (*cf.* Figure 2).

Koch and Ladd [4] determined k_2 for concentrated arrays by using a lubrication theory. It was necessary to solve not only the leading-order equations (10) but also the next two equations of the expansion in the Reynolds number. This calculation is labourious for Newtonian fluids, and with the nonlinear viscous terms for power-law fluids in mind we have not pursued a full lubrication theory for non-zero Reynolds numbers. An order-of-magnitude analysis is straightforward though. As argued in [1], $V_1^{(0)}$ is $O(U/\epsilon)$ when the mean flow is in the 1-direction, where ϵa is the size of the gap between the cylinders; $V_2^{(0)}$ is $O(U/\epsilon^{1/2})$. Spatial derivatives perpendicular to the gap scale with $a\epsilon$ whereas those aligned with the gap scale with $a\epsilon^{1/2}$. The left-hand side of (11) is thus $O(\epsilon^{-5/2})$. From (11), $V_1^{(1)}$ can be shown to be $O(\epsilon^{2n-5/2})$ and $P^{(1)}$ $O(\epsilon^{-2})$. In the next step of the expansion, the $O(\mathrm{Re}^2)$ momentum equation, the inertial term is then $O(\epsilon^{2n-4})$, so that $P^{(2)}$ is $O(\epsilon^{2n-7/2})$. The first contribution from inertia to the drag coefficient is of the same order, so that we finally have,

$$k_2(\phi, n, \theta) \sim \left(1 - (\phi/\phi_{\max})^{1/2}\right)^{2n-7/2}, \qquad \phi_{\max} - \phi \ll 1, \tag{13}$$

where $\phi_{\max}$ is the maximum solid fraction ($\pi/4$ for square arrays, $\pi/(2\sqrt{3})$ for hexagonal arrays). The proportionality constant may depend on n and θ, but not on ϕ (to leading order in $\phi_{\max} - \phi$) and a full lubrication theory would be required for its determination.

Koch and Ladd [4] also determined k_2 analytically for flow of Newtonian fluids through dilute arrays by using the point-force approximation. Their result is

$$k_2\phi = \frac{0{\cdot}0286}{b^2} - \frac{0{\cdot}0348}{b^3} + \frac{0{\cdot}0146}{b^4}, \tag{14}$$

with $b = \log\phi^{-1/2} - 0{\cdot}738$. We shall use this result below to obtain an approximation for power-law fluid flow.

2.2. Numerical results for on-axis flows

The values of k_2 at various area fractions and power-law indices have been obtained by calculating the drag coefficient at several Reynolds numbers and then applying a least squares regression analysis. Typically, flows at five different Reynolds numbers were simulated and a second-order polynomial in the square of the Reynolds number was used to fit the data. The Reynolds number was not an input parameter of the problem; in each simulation a pressure drop over the unit cell was prescribed and the resulting averaged velocity in the cell was calculated (C_d was then obtained from (5)).

Figure 3 shows k_2 for on-axis flows through square arrays as a function of area fraction for $n = 0{\cdot}5$, 1 and 1·5. Also shown are numerical simulation results in [4] for $n = 1$, with which the present results are seen to agree. A very pronounced dependence of k_2 on both the solid area fraction and the power-law index is observed.

As discussed in [1], the variation of the drag coefficient with n depends of course on the way in which the drag coefficient is defined in the first place. The main dependence of k_0 on the power-law index was shown in [1] to be caused by scaling the viscosity in (5) with the cylinder radius and the averaged velocity in the array. A new drag coefficient $\tilde{C}_d$ was introduced that does not depend on n:

$$F(\mathrm{Re} = 0) \;=\; \tilde{C}_d(\phi, \mathrm{Re} = 0)\eta_L U, \tag{15}$$

where $\eta_L \equiv K(U_L/L)^{n-1}$; $U_L = Uc/L$ with c half the distance between the cylinder centres. $L(\phi, n)$ is defined such that $\tilde{C}_d$ does not depend on n (essentially the n-dependence is absorbed by the lengthscale $L(\phi, n)$). It was shown, however, that L is almost independent of n and we presented the n-averaged value $\mathcal{L}(\phi)$ for flows through several geometries. Assuming that L is independent of n and comparing (15) with (5) then yielded an explicit expression for the dependence of C_d on the power-law index,

$$C_d(\phi, n, \mathrm{Re} = 0) \approx C_d(\phi, 1, \mathrm{Re} = 0) \left(\frac{\phi}{\phi_{\max}}\right)^{(1-n)/2} \left(\frac{\mathcal{L}}{a}\right)^{2-2n}, \tag{16}$$

where $\mathcal{L}$ can be approximated by the half of the size of the gap between the cylinders.

The same argument can be used for the inertial contribution to C_d: we would expect k_2 to depend strongly on n because of the choice of lengthscale (the cylinder radius) in (5). We shall therefore consider the extension of (15) to finite Reynolds numbers and write

$$\tilde{C}_d(n, \phi, \mathrm{Re}) = \tilde{k}_0 + \tilde{k}_2 \mathrm{Re}^2 + ..., \tag{17}$$

where $\tilde{k}_2 = (\mathcal{L}(\phi)/a)^{2n-2} (\phi_{\max}/\phi)^{(1-n)/2} k_2$. It is shown in [1] that $\tilde{k}_0$ does not depend significantly on the power-law index; we shall now investigate the dependence of $\tilde{k}_2$ on n. However, we still expect this dependence to be significant, because the choice of lengthscale arises again in the definition of the Reynolds number. We therefore introduce a new Reynolds number $\widehat{\mathrm{Re}} = \rho a U/\eta_H$, in which the viscosity scale $\eta_H \equiv K(U_H/H)^{n-1}$ is based on a length scale $H(\phi, n)$ and a velocity scale $U_H = Uc/H$ (where $2c$ is the dimension of the unit cell), which will be chosen below,

$$\widehat{\mathrm{Re}} = \left(\frac{H(\phi, n)}{a}\right)^{2n-2} \left(\frac{\phi_{\max}}{\phi}\right)^{(1-n)/2} \mathrm{Re}. \tag{18}$$

The dependence on ϕ arises from the ratio $c/a = \phi_{\max}/\phi$. The inertial correction ($\tilde{k}_2 \mathrm{Re}^2$) in (17) is now written as $\widehat{k}_2 \widehat{\mathrm{Re}}^2$. The coefficient $\widehat{k}_2$ is related to k_2 through

$$\widehat{k}_2 = \left(\frac{\mathcal{L}(\phi)}{a}\right)^{2n-2} \left(\frac{H(\phi, n)}{a}\right)^{4-4n} \left(\frac{\phi_{\max}}{\phi}\right)^{(n-1)/2} k_2. \tag{19}$$

We shall now define $H(\phi, n)$ such that $\widehat{k}_2(\phi, n)$ does not depend on n. We can obtain $H(\phi, n)$ from the simulation results through

$$\frac{H(\phi, n)}{a} = \left(\frac{k_2(\phi, n)}{k_2(\phi, 1)}\right)^{1/(4n-4)} \left(\frac{\phi_{\max}}{\phi}\right)^{1/8} \left(\frac{\mathcal{L}(\phi)}{a}\right)^{1/2}. \tag{20}$$

H/a decreases very strongly with increasing area fraction, so in Figure 4 we show results for H/L_g instead, where $L_g = ((\phi_{\max}/\phi)^{1/2} - 1)a$ is half the minimum gap size between the cylinders. The results are shown together with those for $\mathcal{L}/L_g$. Both H and $\mathcal{L}$ are almost proportional to L_g. However H/L_g, unlike $\mathcal{L}/L_g$, does show some dependence on the power-law index, especially at intermediate area fractions. It is also seen from Figure 4 that H is larger, and $\mathcal{L}$ smaller, than the gap dimension L_g. Substitution of (13), together with the lubrication theory for $\mathcal{L}/a$ from [1], in the right-hand side of (20) shows that at large ϕ, $H/a \sim (\phi/\phi_{\max})^{1/4}$, but the proportionality factor is a power of the corresponding factor in (13), which is expected to depend on n. Therefore, we cannot use (13) to determine the

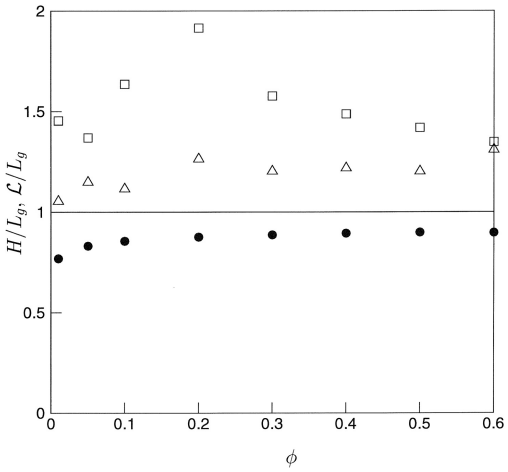

Figure 4. Length scale H which is used in the scaling of the Reynolds number to obtain a dimensionless inertial contribution to the drag that is independent of the power-law index. H has been made dimensionless with half the minimum gap size between the cylinders $L_g = ((\phi_{\max}/\phi)^{1/2} - 1)a$. (□), $n = 0{\cdot}5$; (△), $n = 1{\cdot}5$. The filled circles show the length scale $\mathcal{L}$ which yields a drag coefficient for creeping flows that is independent of n.

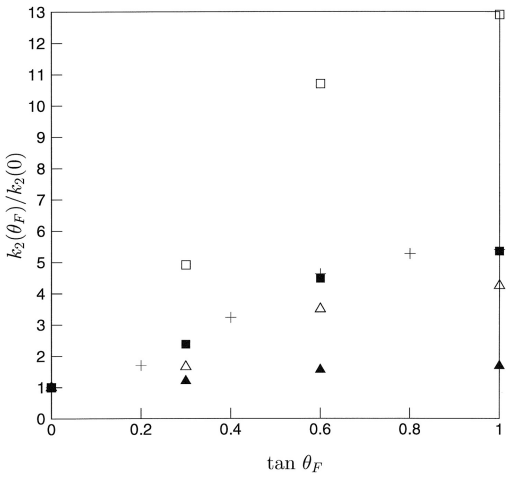

Figure 5. Variation of k_2 with the angle θ_F that the applied force makes with an axis of the array for power-law fluids ($n = 0{\cdot}5$, open symbols) and Newtonian fluids (filled symbols) for solid area fractions: (□), $\phi = 0{\cdot}1$, (△), $\phi = 0{\cdot}3$. Also shown are Koch and Ladd's [4] results (+) for $\phi = 0{\cdot}1$, $n = 1$.

applicability of a scaling argument beyond the range of n simulated. But for $\phi \geq 0{\cdot}6$, no significant dependence on n should be expected for $0{\cdot}5 \leq n \leq 1{\cdot}5$.

We have used (20) (with H approximated by L_g) and (14) to obtain an approximation to k_2 for power-law fluid flow through dilute arrays; the result is shown in Figure 3. For $n = 1{\cdot}5$ this works very well; for $n = 0{\cdot}5$ close inspection shows that the results do converge to this approximation, but only slowly.

2.3. Off-axis flows

For creeping flows of Newtonian fluids the drag coefficient is independent of flow direction and the drag force is aligned with the averaged fluid velocity. In [1] a small dependence of the drag coefficient on flow direction (a few percent) was found for creeping flows of shear-thinning fluids. Also, the averaged fluid velocity was found to be significantly misaligned with the drag force. The correction to the drag coefficient due to inertia has been shown in [4] to exhibit a strong angular dependence for Newtonian fluids and a small misalignment between drag force and averaged fluid velocity was also found. We now investigate the behaviour of shear-thinning fluids in this case.

In Figure 5 results are presented for the ratio of k_2 for off-axis flows of shear thinning fluids ($n = 0{\cdot}5$) and its corresponding on-axis value. θ_F is the angle between the drag force and an axis of the array. Results for shear-thinning fluids ($n = 0{\cdot}5$) and Newtonian fluids show the same trends: at high area fractions, k_2 becomes independent of θ_F, whereas at low values of

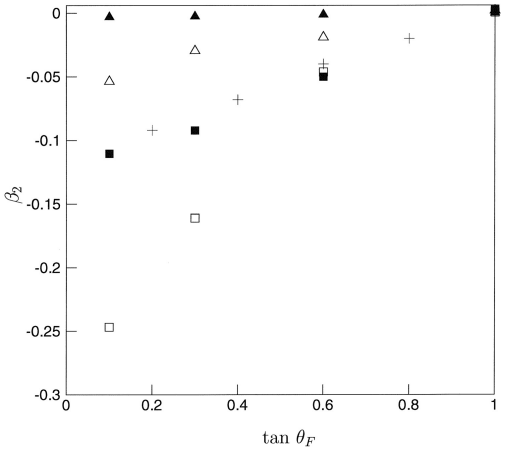

Figure 6. First inertial contribution β_2 to the ratio $\tan\theta/\tan\theta_F$ as a function of the angle θ_F that the applied force makes with an axis of the array for power-law fluids ($n = 0{\cdot}5$, open symbols) and Newtonian fluids (filled symbols) for solid area fractions: (□), $\phi = 0{\cdot}1$, (Δ), $\phi = 0{\cdot}3$. Results for $n = 1$ at $\phi = 0{\cdot}1$ by Koch and Ladd [4] are indicated by +.

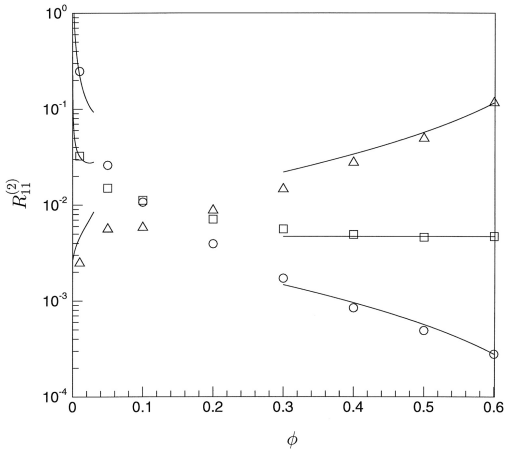

Figure 7. Dimensionless inertial contribution to the dimensionless velocity variance, $R_{11}^{(2)}$ (defined in (23)), as a function of the solid area fraction ϕ at different values of the power-law index: (Δ), $n = 0{\cdot}5$; (□), $n = 1$ and (◯), $n = 1{\cdot}5$. The lines at large solid fraction are the lubrication scaling (27), where we have used the numerical simulation result at $\phi = 0{\cdot}6$ to obtain the proportionality constant. The lines at low ϕ correspond to the asymptotic result (26) for Newtonian fluids; for power-law fluids the result based on (29) is shown, with $\mathcal{Z}_{ij} = L_g$ using $R_{ij}^{(2)}(\phi, n = 1)$ from (26).

ϕ, k_2 becomes much larger for off-axis flows. This trend at low ϕ is even more pronounced for shear-thinning fluids than it is for Newtonian fluids.

In Figure 6 the first inertial contribution to the misalignment between the drag force and the averaged velocity is shown. For creeping flows of shear-thinning fluids it is shown in [1] that the averaged velocity is more aligned with the nearest axis of the array than the drag force for $\phi = 0{\cdot}3$, while the opposite is true for $\phi = 0{\cdot}1$. Denoting the angle between the superficial fluid velocity and the nearest axis of the array by θ, and the angle between the drag force and the same axis of the array by θ_F, we define

$$\tan\theta = \left[\beta_0(n, \phi, \theta_F) + \beta_2(n, \phi, \theta_F)\mathrm{Re}^2 + ...\right]\tan\theta_F. \tag{21}$$

The results for β_0 have been presented in [1]; β_2 as a function of θ_F is shown in Figure 6 for different solid area fractions, for shear-thinning fluids ($n = 0{\cdot}5$) and Newtonian fluids. All results for β_2 are negative, making the averaged fluid velocity more aligned with an axis of the array than for creeping flows. We see that the results for shear-thinning fluids are qualitatively similar to those for Newtonian fluids (both for the drag coefficient and the direction of the averaged fluid velocity). Although this suggests a straightforward relation between these results, the length scale that would have been required in the definition of the Reynolds number (in (21)) to (potentially) eliminate the dependence on power-law index does depend on flow direction and is not the same as $\mathcal{L}$ or H.

3. First effects of inertia on velocity variances

The velocity variance tensor for on-axis flow (in the x_1-direction) through a periodic array is written as

$$\overline{v_i v_j} \equiv \overline{(V_i - \overline{V}_i)(V_j - \overline{V}_j)} \equiv R_{ij}(\phi, n, \mathrm{Re})\, \overline{V}_1{}^2, \tag{22}$$

where an overbar denotes the average over the unit cell. The dependence on Reynolds number of R_{ij} at small values of Re can be determined from the Taylor-series expansions (8) used in Section 2.1. The $O(\mathrm{Re})$ contribution to the velocity variance vanishes because the correction to the velocity field of that order is an odd function of position. A similar argument holds for higher order terms that are odd powers of Re and we can write

$$R_{ij}(\phi, n, \mathrm{Re}) \;=\; R_{ij}^{(0)}(\phi, n) + R_{ij}^{(2)}(\phi, n)\mathrm{Re}^2 + \ldots \tag{23}$$

As with the corresponding expansion for the drag coefficient, (12), our computations confirm (23). In the following we shall present results for $R_{ij}^{(2)}$; the creeping flow velocity variances $R_{ij}^{(0)}$ are presented in [1].

At each area fraction and power-law index we have performed simulations at about five different Reynolds numbers and used a regression analysis to obtain $R_{ij}^{(2)}$. The results for $R_{11}^{(2)}$ are shown in Figure 7 as functions of area fraction at $n = 0{\cdot}5$, 1 and 1·5. All values are positive while the corresponding results for $R_{22}^{(2)}$ were all negative, indicating that the velocity variance in the flow direction increases with Reynolds number whereas the perpendicular component decreases (the flow tends to conform less to the geometry of the cylinders). There is a monotonic decrease with increasing ϕ in these coefficients for Newtonian and shear-thickening fluids, and a monotonic increase for shear-thinning fluids. This is in sharp contrast with the results presented in [1] for $R_{ij}^{(0)}$, which were seen to be virtually independent of n.

For flows of Newtonian fluids through dilute square arrays, the velocity field (and hence $R_{ij}^{(2)}$) can be determined by using the point-force approximation, as discussed in [1] (Section 5.1). The Fourier coefficient of the fluid velocity disturbance for dimensionless wavenumber $\mathbf{k}$ is (see [1, Equation (25)]), in the Oseen approximation [4],

$$\hat{\mathbf{v}}(\mathbf{k}) = \sum_{k\neq 0} \frac{\mathbf{F}\cdot\left(\mathbf{I} - \mathbf{kk}/k^2\right)}{\mu(2\pi k)^2 + 4\pi i \rho c \mathbf{k}\cdot\mathbf{U}}, \tag{24}$$

where c is the half spacing between the cylinders in a square array, and the summation is over all the vectors of the reciprocal lattice. The dimensionless velocity variance components can be expressed as single summations over wavenumber space,

$$R_{ij} = \overline{V}_1{}^{-2} \sum_{k\neq 0} \hat{v}_i(\mathbf{k})\hat{v}_j(-\mathbf{k}). \tag{25}$$

The resulting summations were carried out numerically, resulting in

$$R_{11}^{(2)} = \frac{0{\cdot}171 k_2}{b} - \frac{5{\cdot}62\times 10^{-4}}{\phi b^2}, \qquad R_{22}^{(2)} = \frac{0{\cdot}0232 k_2}{b} - \frac{5{\cdot}62\times 10^{-4}}{\phi b^2}, \tag{26}$$

where k_2 is given by (14) and $b = \log\phi^{-1/2} - 0{\cdot}738$. The numerical simulation results are seen to tend to this asymptotic result for Newtonian fluids for small values of ϕ.

Also shown in Figure 7 are order-of-magnitude estimates from a lubrication scaling. As mentioned above, we have not pursued a full lubrication theory (which would only yield the proportionality constants) because of the highly nonlinear nature of the equations of motion. Furthermore, a lubrication theory for the transverse velocity variance is not feasible; it can be shown that its main contribution does not come from the narrow gap between the cylinders, but from just outside the gap. For concentrated arrays the first terms in the expansion (8) for the dimensionless velocity V_1^* in the narrow gap between the cylinders are: $V_1^{(0)}$, which is $O(\epsilon^{-1})$; $V_1^{(1)}$, which is $O(\epsilon^{2n-5/2})$ and $V_1^{(2)}$, which is $O(\epsilon^{3n-7/2})$ (of course, $\overline{V}_1^*$ is by definition equal to unity for on-axis flow). The most significant contribution to $R_{11}^{(2)}$, $O(\epsilon^{3n-3})$, is thus found to arise from $V_1^{(0)}V_1^{(2)}$ if $n > 0{\cdot}5$:

$$R_{11}^{(2)}(\phi, n) \sim \left(1 - (\phi/\phi_{\max})^{1/2}\right)^{3n-3} \qquad \phi_{\max} - \phi \ll 1. \tag{27}$$

In Figure 7 the agreement of the numerical results with this expression is seen to be good.

The strong dependence of $R_{ij}^{(2)}$ on the power-law index is affected by the definition of the Reynolds number. As with the drag coefficient, we can define a Reynolds number $\mathrm{Re}' \equiv \rho a U/\eta_Z$, where $\eta_Z \equiv K(U_Z/Z)^{n-1}$ is the viscosity scale based on a length scale $Z(\phi, n)$ and a velocity $U_Z \equiv Uc/Z$, and rewrite the expansion (23) as $R_{ij}(\phi, n, \mathrm{Re}') = R_{ij}^{(0)}(\phi, n) + R_{ij}^{'(2)}(\phi, n)\mathrm{Re}'^2 + \ldots$. We define Z_{ij} such that $R_{ij}^{'(2)}$ is independent of n. This results in

$$Z_{ij}(\phi, n)/a = \left(\frac{\phi_{\max}}{\phi}\right)^{1/4} \left(\frac{R_{ij}^{(2)}(\phi, n)}{R_{ij}^{(2)}(\phi, 1)}\right)^{1/(4n-4)}. \tag{28}$$

In Figure 8 we have plotted the ratio $Z_{ij}(\phi, n)/L_g$. Most of the values are somewhat larger than half the minimum gap size (the solid line in Figure 8). The value of Z_{ij} can therefore be replaced by the n-averaged value, denoted by $\mathcal{Z}_{ij}$. The dependence of $R_{ij}^{(2)}$ on the power-law index is then given by

$$R_{ij}^{(2)}(\phi, n) = R_{ij}^{(2)}(\phi, 1) \left(\frac{\phi}{\phi_{\max}}\right)^{n-1} \left(\frac{\mathcal{Z}_{ij}(\phi)}{a}\right)^{4n-4}, \tag{29}$$

where $\mathcal{Z}_{ij}$ can be approximated by half the gap between the cylinders. In Figure 7 we have combined (29) with (26) to obtain the behaviour of $R_{11}^{(2)}$ at small ϕ expected from this argument. This is seen to give a good approximation to the behaviour at small ϕ.

4. Moderate Reynolds number flows

4.1. Drag coefficient

The results presented so far have been for the first effects of inertia at small but finite Reynolds numbers. In Figure 9 the drag coefficient is presented for a much wider range of Reynolds numbers, for solid fraction $\phi = 0{\cdot}3$. Results for flow along the diagonal symmetry axis $\theta_F = \pi/4$ are shown in Figure 10. The results for $n = 0{\cdot}5$ and $n = 1{\cdot}5$ are seen to be qualitatively very similar to the results for Newtonian fluids. The drag coefficient increases according to (12) only at small Reynolds numbers. At intermediate Reynolds numbers, the increase of C_d with Re is more linear, and relatively small for on-axis flows. The drag force for on-axis flows

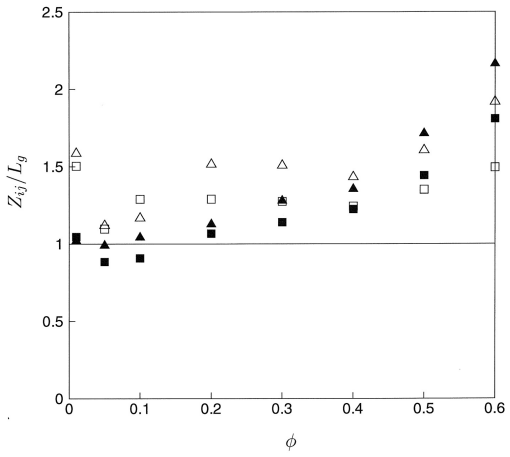

Figure 8. Variation of the length scale Z_{ij}, defined by (28), with solid area fraction ϕ, for power-law coefficients $n = 0{\cdot}5$ (open symbols) and $n = 1{\cdot}5$ (filled symbols). Z_{ij} has been made dimensionless with half the minimum gap size between the cylinders $L_g = ((\phi_{\max}/\phi)^{1/2} - 1)a$. (□), Z_{11}; (Δ), Z_{22}.

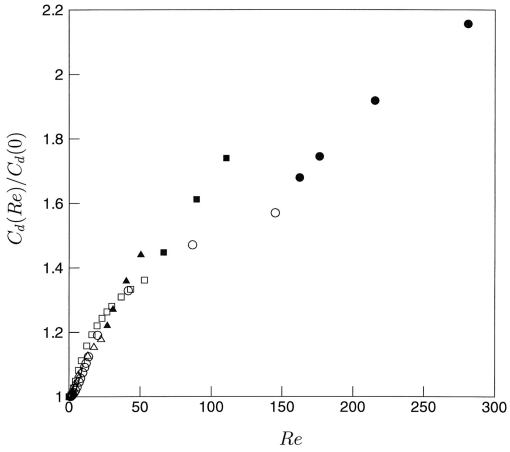

Figure 9. Variation of drag coefficient with Reynolds number for on-axis, moderate Reynolds number flows at solid area fraction $\phi = 0{\cdot}3$: (Δ), power-law fluid with $n = 0{\cdot}5$; (□), $n = 1$; (◯), $n = 1{\cdot}5$. Filled symbols represent time-averaged values in unsteady flow.

is expected to be smaller than for off-axis flows because each cylinder is shielded by another one directly upstream.

Beyond a critical Reynolds number the flow becomes unsteady: the time signals go through a sequence of period-doubling bifurcations [4]. In most cases presented here P2-oscillations were observed; P4-oscillations occurred only at some of the largest Reynolds numbers studied here. For these unsteady cases the drag coefficient and Reynolds number are based on the time-averaged superficial fluid velocity (the force is held constant). The value of the critical Reynolds number (denoted by Re_c) increases with n. A significant contribution to this dependence on n is caused by the choice of the viscosity scale in the definition of Re. The results presented in the previous section suggest that any dependence on power-law index will be minimal when using the Reynolds number $\widehat{\mathrm{Re}}$ (defined by (18)) with $H/a = L_g/a = (\phi_{\max}/\phi)^{-1/2} - 1$. That is, by using a viscosity scale that is more appropriate for the flow through the narrow gap between the cylinders. In Table 1 the values of Re_c and $\widehat{\mathrm{Re}}_c$ are shown. Clearly, $\widehat{\mathrm{Re}}_c$ is virtually the same for shear-thinning and Newtonian fluids. For shear-thickening fluids ($n = 1{\cdot}5$) the transition to unsteady flow occurs only at a somewhat larger Reynolds number than expected from this scaling argument.

For on-axis flows, but not for the off-axis flows studied here, the drag coefficient is seen to increase sharply beyond the critical Reynolds number. In the unsteady regime the form drag is substantial due to the shedded recirculation zones, causing the drag force to be of $O(\rho a U^2)$ such that the drag coefficient becomes a linear function of Reynolds number [4]. For off-axis flows, the drag follows the same scaling even in steady flow, indicating that the form drag is already significant. This is found not because of wake formation (which happens only just before the onset of unsteady flow) but is caused by the strong curvature of the streamlines.

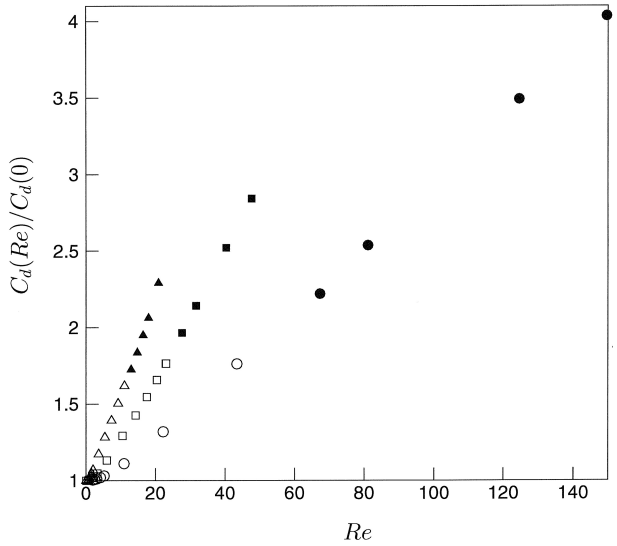

Figure 10. Variation of drag coefficient with Reynolds number for off-axis, moderate Reynolds number flows at solid area fraction $\phi = 0{\cdot}3$, with mean flow along the symmetry axis $\theta_F = \pi/4$. (Δ), power-law fluid with $n = 0{\cdot}5$; (□), $n = 1$; (◯), $n = 1{\cdot}5$. Filled symbols represent time-averaged values in unsteady flow.

Table 1. Critical Reynolds number Re_c beyond which the flow is unsteady

ϕ	n	Re_c ($\theta_F = 0$)	Re_c ($\theta_F = \pi/4$)	$\widehat{\mathrm{Re}}_c$ ($\theta_F = 0$)	$\widehat{\mathrm{Re}}_c$ ($\theta_F = \pi/4$)
0.3	0.5	22.5–26.9	11.0–13.0	46.3–55.4	22.7–26.7
	1	53.0–66.4	23.7–27.6	53.0–66.4	23.7–27.6
	1.5	145–162	43.45–81.1	70.5–78.9	21.1–32.7
0.5	0.748	31.6–48		66.8–102	
	0.83	43.6–58.3		72.3–96.6	
	1	78.2–95.1		78.2–95.1	

Experimental data for flows through tube banks at moderate Reynolds numbers have been presented for Newtonian fluids by Bergelin [11, 12] and for inelastic non-Newtonian fluids by Adams and Bell [8]. The same tube banks were used in both studies. An attempt to develop a model for power-law fluid flows through tube banks was made by Prakash [9].

Amongst the tube arrangements that were studied, one was a square array with ten rows of tubes and solid area fraction $\phi = 0{\cdot}50$. The experimental data presented for this case, with $n = 1$, $0{\cdot}83$ and $0{\cdot}748$, are shown in Figure 11 together with the corresponding numerical simulation results. Also shown are Ghaddar's [3] numerical simulation results for $n = 1$, with which our results are seen to agree well. Despite the significant scatter in the experimental data, they appear to follow the same trends as the numerical simulation results. The drag coefficients determined in the experiments are consistently somewhat larger than the computed values for both power-law and Newtonian fluids and by about the same amount in each case.

There are several possible explanations for the observed differences. Antonopoulos and Gosman [13] presented numerical simulations for flows of Newtonian fluids through arrays of cylinders for a range of Reynolds numbers. They considered the flow through a large number

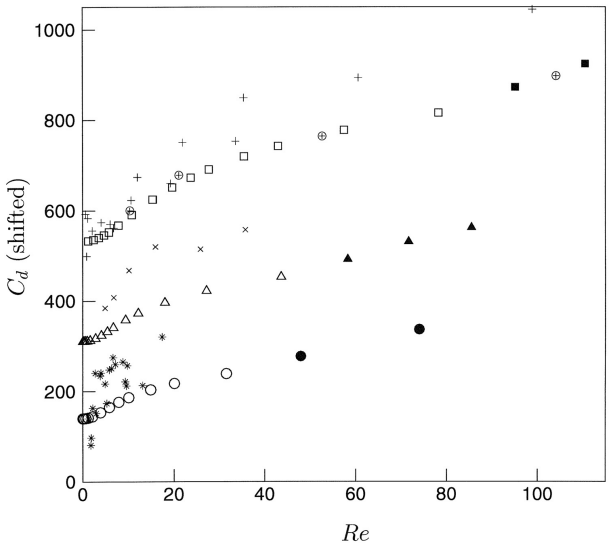

Figure 11. Drag coefficient C_d versus Reynolds number for on-axis flows at moderate Reynolds number with solid area fraction $\phi = 0{\cdot}5$. For clarity of presentation, the results for $n = 0{\cdot}748$ have been shifted downwards by 100 units. (□), Newtonian fluid; (△), $n = 0{\cdot}83$; (◯), $n = 0{\cdot}748$; (⊕), numerical simulation results by Ghaddar [3] for $n = 1$; (+), experimental results by Bergelin *et al.* [11] for $n = 1$; (×), experimental results by Adams and Bell [8] for $n = 0{\cdot}83$; (∗), experimental results by Adams and Bell [8] for $n = 0{\cdot}748$. Filled symbols represent time-averaged values in unsteady flow.

of rows of cylinders and showed that the number of rows used by Bergelin *et al.* [11] was not sufficient to eliminate entrance effects. Although the local pressure drop over each row hardly changed beyond the third row of cylinders, the averaged pressure drop over the entire bank required a far larger number of rows for convergence. This is caused by the pressure drop over the initial row being larger than the fully-developed value by up to 50%, which is enough to explain most of the discrepancy between experimental and simulation data in Figure 11.

Although it is difficult to be certain, the discrepancy does appear to increase with Reynolds number. A further caution for comparing the simulation results with experimental data is that three-dimensional flow structures develop near the side walls of the banks, which shorten the effective length of the tubes, thereby increasing the drag coefficient. Also, the Reynolds number of the flow based on the dimensions of the tube bank is of $O(15\mathrm{Re})$, which may be large enough for the velocity profile at the inlet to be significantly non-uniform. Some degree of preferential flow could occur, or the flow could have become non-spatially-periodic due to advection of vorticity through the tube bank.

The observed discrepancy between experiments and simulations would not have been visible had the results been presented in the same format as that adopted in [8, 11, 12]. The experimental data were presented originally in terms of a friction factor f, in an attempt to correlate the data for different fluids. As the friction factor varies strongly with Reynolds number (roughly as the inverse), experimental data for tube banks are usually presented in log-log graphs. Consequently, the detailed variation visible in Figure 11 is masked by the strong trend of $f \sim \mathrm{Re}^{-1}$.

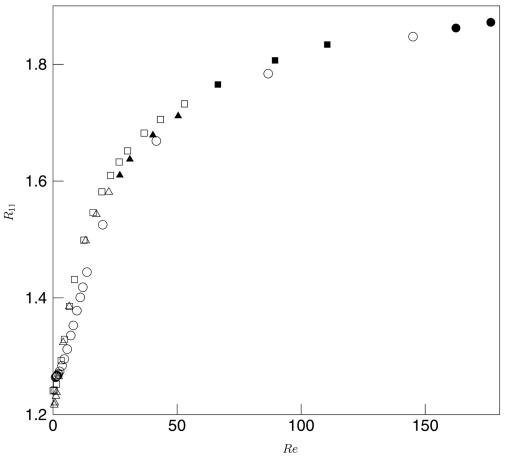

Figure 12. Dimensionless velocity variance component in the main flow direction, R_{11}, as a function of the Reynolds number Re for on-axis flow at solid area fraction $\phi = 0{\cdot}3$; (Δ), $n = 0{\cdot}5$; (□), $n = 1$; (◯), $n = 1{\cdot}5$. Filled symbols represent time-averaged values for unsteady flows.

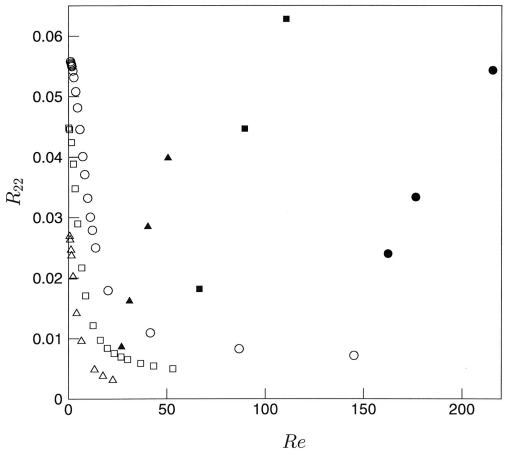

Figure 13. Dimensionless velocity variance component perpendicular to the main flow direction, R_{22}, as a function of Reynolds number Re for solid area fraction $\phi = 0{\cdot}3$. (□), on-axis flow of Newtonian fluid; (Δ), on-axis flow of power-law fluid with $n = 0{\cdot}5$; (◯), $n = 1{\cdot}5$. Filled symbols represent time-averaged values for unsteady flows.

4.2. VELOCITY VARIANCES

The dimensionless velocity variance R_{11} is shown in Figure 12 for on-axis flow ($n = 0{\cdot}5$, 1 and $1{\cdot}5$) at solid fraction $\phi = 0{\cdot}3$. For cases in which the flow was unsteady we have taken the averages in the definition (22) over time as well as space. As with the drag coefficient, the dependence of R_{11} on Reynolds number for power-law fluids is quantitatively very similar to that for Newtonian fluids. A monotonic increase of R_{11} with Re is seen that is hardly affected by the transition to unsteady flow.

The corresponding results for R_{22} are shown in Figure 13. As expected, in the range of Re for which the flow is steady, R_{22} simply decreases as Re is increased. In the unsteady regime this normal velocity variance suddenly increases, but is still much smaller than the value of R_{11}, indicating that although the recirculation zone between the cylinders becomes stronger, the flow through the channels between the rows of cylinders is not strongly affected.

Results for off-axis flows at the symmetry angle ($\theta_F = \pi/4$) are shown in Figure 14. In this case R_{11} decreases initially with increasing Reynolds number, but this trend is reversed at moderate Re. As with the other off-axis flow results, there is no significant change in the trend at the transition to the unsteady regime. On the other hand, R_{12} almost levels off after the transition to unsteady flow. All the results for flows at moderate Reynolds numbers of power-law fluids with $n = 0{\cdot}5$ or $1{\cdot}5$ are qualitatively similar to the results for Newtonian fluids.

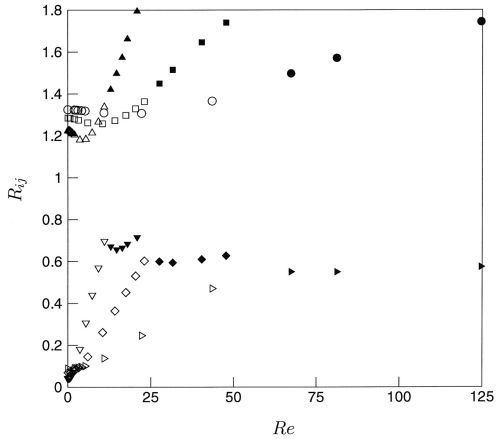

Figure 14. Dimensionless velocity variance components R_{ij} as functions of Reynolds number Re for off-axis flow at the symmetry angle ($\theta_F = \pi/4$) at solid area fraction $\phi = 0{\cdot}3$. R_{11}: (Δ), $n = 0{\cdot}5$; ($\square$), $n = 1$; ($\bigcirc$), $n = 1{\cdot}5$. R_{12}: (∇), $n = 0{\cdot}5$; ($\Diamond$), $n = 1$; ($\triangleright$), $n = 1{\cdot}5$. Filled symbols represent time-averaged values for unsteady flows.

5. Summary and conclusions

Numerical results have been presented for flows with inertia of inelastic non-Newtonian fluids through square arrays of cylinders, using the truncated power-law fluid model. We have shown that the inertial correction to the drag coefficient at small Reynolds numbers is quadratic in the Reynolds number (*cf.*(12)). Results for the proportionality factor k_2 of the first inertial contribution have been presented for on-axis and off-axis flows. The dependence of k_2 on the power-law index for on-axis flows is shown to be caused mainly by the choice of length scale in the definition of the Reynolds number. This is consistent with the results presented in [1]. At small Reynolds numbers, the first inertial contribution to the velocity variances is of the form (23) for on-axis flows. As with the drag coefficient, the strong dependence of the proportionality factor (multiplying the square of the Reynolds number) on the power-law index is essentially due to the choice of length scale in the definition of the Reynolds number.

At larger Reynolds numbers the drag coefficient increases with Reynolds number at a lower than quadratic rate (approximately linearly for off-axis flow), up to the critical Reynolds number, beyond which no stable steady solution is found. In the unsteady regime the drag is dominated by form drag, and the drag coefficient is approximately linearly dependent on Re. The value of the critical Reynolds number for power-law fluids depends on the power-law index; scaling analysis shows how to relate the critical Reynolds number for a power-law fluid to that for a Newtonian fluid. The velocity variances for Newtonian and shear-thinning fluids are qualitatively similar functions of the Reynolds number throughout the Reynolds number regime considered here.

Comparison of the simulation results for the drag coefficient with the experimental data of Bergelin *et al.* [11, 12] and Adams and Bell [8] shows good agreement, although the latter are somewhat larger than the former, which may be caused (as suggested in [13]) by entrance effects in the experiments. The dependence of the drag coefficient on the Reynolds number is not entirely clear in the experimental data because of the significant scatter in the data.

Acknowledgements

This work has been made possible by a grant from the EPSRC (GR/M 39572) and has been supported by QinetiQ, Vosper Thornycroft, Dowty Aerospace Propellers, AEA Technology and BAE Systems. We would like to thank Mr. Li Ding and Prof. Robert L. Street of Stanford University and Prof. C. Pozrikidis of the University of California at San Diego for valuable discussions. The authors gratefully acknowledge the computer facilities provided under EPSRC grant GR/L86821.

References

1. P.D.M. Spelt, T. Selerland, C.J. Lawrence and P.D. Lee, Flows of inelastic non-Newtonian fluids through arrays of aligned cylinders. Part 1. Creeping flows. Submitted to *J. Eng. Math.* (2005) 57–80.
2. D.A. Edwards, M. Shapiro, P. Bar-Yoseph and M. Shapira, The influence of Reynolds number upon the apparant permeability of spatially periodic arrays of cylinders. *Phys. Fluids A* 2 (1990) 45–55.
3. C.K. Ghaddar, On the permeability of unidirectional fibrous media: a parallel computational approach. *Phys. Fluids* 7 (1995) 2563–2586.
4. D.L. Koch and A.J.C. Ladd, Moderate Reynolds number flows through periodic and random arrays of aligned cylinders. *J. Fluid Mech.* 349 (1997) 31–66.
5. C.C. Mei and J.-L. Auriault, The effect of weak inertia on flow through a porous medium. *J. Fluid Mech.* 222 (1991) 647–663.
6. R.B. Bird, R.C. Armstrong, and O. Hassager, *Dynamics of Polymeric Liquids. Vol. 1: Fluid Mechanics*. New York: John Wiley (1987) 649 pp.
7. S.J.D. D'Alessio and J.P. Pascal, Steady flow of a power-law fluid past a cylinder. *Acta Mech.* 117 (1996) 87–100.
8. D. Adams and K.J. Bell, Fluid friction and heat transfer for flow of sodium carboxy methylcellulose solutions across banks of tubes. *Chem. Eng. Prog. Symp. Ser.* 64 (1968) 133–145.
9. O. Prakash, S.N. Gupta and P. Mishra, Newtonian and inelastic non-Newtonian flow across tube banks. *Ind. Eng. Chem.* 26 (1987) 1365–1372.
10. D.V.N. Prasad and R.P. Chhabra, An experimental investigation of the cross-flow of power-law liquids past a bundle of cylinders and in a bed of stacked screens. *Can. J. Chem. Eng.* 79 (2001) 28–35.
11. O.P. Bergelin, G.A. Brown, H.L. Hull and F.W. Sullivan, Heat transfer and fluid friction during viscous flow across banks of tubes – III. A study of tube spacing and tube size. *Trans. ASME* 72 (1950) 881–888.
12. O.P. Bergelin, G.A. Brown and S.C. Doberstein, Heat transfer and fluid friction during viscous flow across banks of tubes – IV. A study of the transition zone between viscous and turbulent flow. *Trans. ASME* 74 (1952) 953–960.
13. K.A. Antonopoulos and A.D. Gosman, The predicition of laminar inclined flow through tube banks. *Comp. Fluids* 14 (1986) 171–180.